Structural and magnetic short-range order in fluorite Yb_{2}TiO_{5}

Jacob Shamblin, Zhiling Dun, Minseong Lee, Steve Johnston, Eun Sang Choi, Katharine Page, Yiming Qiu, and Haidong Zhou

Phys. Rev. B **96**, 174418 — Published 14 November 2017

DOI: 10.1103/PhysRevB.96.174418

Structural and magnetic short range order in fluorite Yb_2TiO_5

Jacob Shamblin,[1,2] Zhiling Dun,[1] Minseong Lee,[3] Steve Johnston,[1] Eun Sang Choi,[3,4] Katharine Page,[5] Yiming Qiu,[6] and Haidong Zhou[1,4,*]

[1]*Department of Physics and Astronomy, The University of Tennessee, Knoxville, Tennessee 37996, USA*
[2]*Department of Nuclear Engineering, The University of Tennessee, Knoxville, Tennessee 37996, USA*
[3]*Florida State University, Department of Physics, Tallahassee, Florida 32306, USA*
[4]*Florida State University, National High Magnet Field Laboratory, Tallahassee, Florida 32310, USA*
[5]*Chemical and Engineering Materials Division, Spallation Neutron Source, Oak Ridge National Laboratory, Oak Ridge, Tennessee 37831, USA*
[6]*NIST Center for Neutron Research, Gaithersburg, Maryland, 20899-6102, USA*

(Dated: October 23, 2017)

We studied structural and magnetic ordering in Yb_2TiO_5 using synchrotron X-ray diffraction, neutron diffraction/total scattering, *ac*/*dc* susceptibility, and inelastic neutron scattering. Diffraction measurements reveal an average disordered fluorite structure with additional diffuse scattering features, which are caused by structural short range orthorhombic order, as evidenced by the neutron pair distribution function measurements. The *ac* susceptibility measurements show a broad peak at $T_f \approx 0.35$ K that displays Arrhenius behavior with an activation energy of 2.51(5) meV. Zero-field neutron scattering measurements show broad magnetic diffuse scattering in the elastic channel with an antiferromagnetic type gapless excitation extending to 1.5 meV. A polarized state with partial spin order is induced with an applied magnetic field which opens a gapped excitation that increases monotonically with field strength.

I. INTRODUCTION

As a result of its geometrical frustration, materials possessing the pyrochlore structure (general formula $A_2B_2O_7$) have come under intense interest due to their complex ground states and exotic excitations[1]. For example, the pyrochlore spin-ices (*e.g.*, $Dy_2Ti_2O_7$ and $Ho_2Ti_2O_7$) have caught the eye of the scientific community due to their zero-point entropy that is strikingly similar to that of cubic water-ice and emergent quasiparticles that behave as magnetic monopoles[2–6]. However, the spin-ice state in these materials is largely classical in nature and much focus has shifted to materials with strong quantum fluctuations. Cations with an effective spin 1/2, such as Yb^{3+}, have been a hot topic of late. Early studies on $Yb_2Ti_2O_7$, demonstrated that although magnetic moments undergo a first order transition into a long-range ordered state at $T_c = 0.24$ K, a fraction of the spin moment remains fluctuating even down to 50 mK[7]. Later, several studied have utilized the spin-wave excitations measurements under magnetic fields to extract the exchange parameters of $Yb_2Ti_2O_7$. The results indicated either a "quantum spin-ice" scenario with the strongest Ising-type interaction J_{zz}[8], or a proximity to an XY antiferromagnet with the strongest "transverse exchange $J_{z\pm}$[9]. It is proposed that the ground state of $Yb_2Ti_2O_7$ is on the border between ordered ferro- and antiferromagnetic states and have suggested that this competition is the root of the quantum spin fluctuations in $Yb_2Ti_2O_7$ rather than spin-ice physics[9–12].

The largest discrepancy among studies on $Yb_2Ti_2O_7$ involves short range order *vs.* long range order. Specific-heat[13], Mössbauer spectroscopy[7], and muon spin relaxation[7] measurements all show a distinct transition at $T_c \approx 0.24$ K. While many studies find no evidence of long range magnetic order associated with this specific-heat anomaly[7,14–16], several neutron diffraction experiments have revealed signatures of long range order in the form of weak magnetic Bragg peaks[17–21]. In studies where no long range magnetic Bragg peaks were observed, the application of even modest magnetic fields ($\mu_0 H = 0.5$ T) induces a transition to long range magnetic order with gapped, dispersive spin wave excitations[8,14]. Controlled studies varying the synthesis technique show that the specific heat anomaly can be significantly broadened by introducing weak amounts of disorder (as little as 1 %) into the crystal structure[22–25]. This sensitivity to disorder is one potential explanation for the controversy around the ground state of $Yb_2Ti_2O_7$.

Strategies for controlling the amount of disorder within a pyrochlore-like sample include partially replacing magnetic A-site cations with nonmagnetic cations (diluted or "dirty" pyrochlore)[26–30] or replacing nonmagnetic B-site cations with additional magnetic cations ("stuffed" pyrochlore)[31,32]. The stuffing procedure specifically (often written as $A^{3+}_{2+x}B^{4+}_{2-x}O^{2-}_{7-x/2}$, summarized in Fig. 1) has three effects: (*i*) additional spins are placed into the lattice, creating more magnetic interactions; (*ii*) at low stuffing levels, the additional A-site cations partially occupy B-sites; and (*iii*) at high stuffing levels, depending on the composition, the pyrochlore ($Fd\bar{3}m$) can degrade into the fully disordered "defect fluorite" structure ($Fm\bar{3}m$, Fig. 1b). This refers to a face-centered cubic unit cell (CaF_2-type) in which the two cations are randomly arranged on a single crystallographic site (4*a*) and oxygen atoms and charge compensating vacancies are randomly arranged on a second crystallographic site (8*c*). For convenience, the end-member of a titanate stuffing series' can be written as A_2TiO_5.

Speaking only on rare-earth compositions, the defect

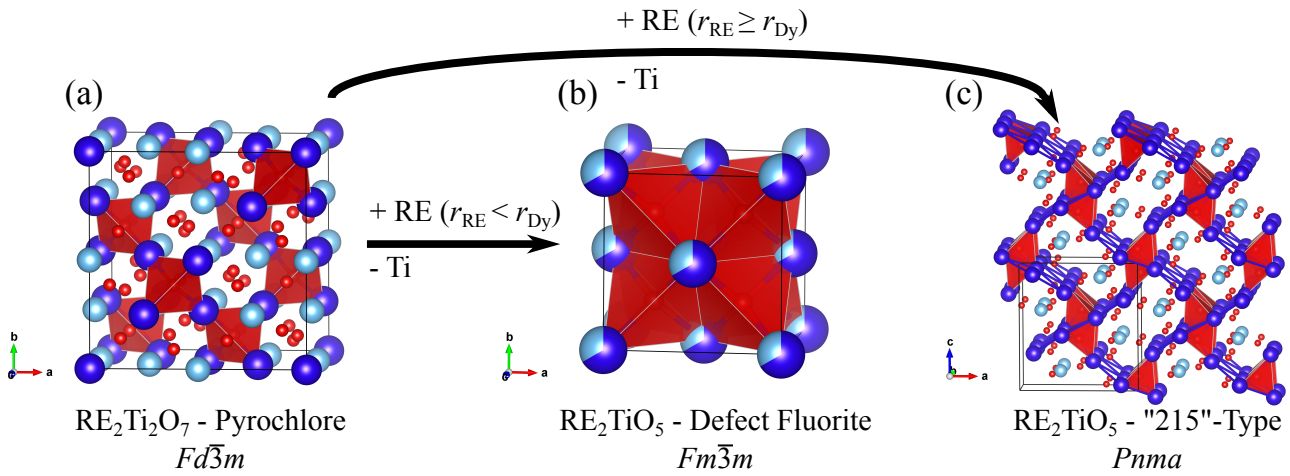

FIG. 1. (color online) Summary of the effect of stuffing additional rare-earth cations (which replace Ti cations) into the pyrochlore structure (a). Blue spheres denote rare-earth (RE) cations, cyan spheres denote Ti cations and red spheres denote oxygen anions. The red polyhedra represent tetrahedra comprised of magnetic, RE cations. For a "fully stuffed" pyrochlore (A_2TiO_5 stoichiometry), when the RE cations are smaller than Dy, the "defect fluorite" structure forms in which the RE and Ti atoms share occupancy of a single site (b). An orthorhombic structure forms at equilibrium with no site mixing when the RE cation is Dysprosium or larger (c).

fluorite structure forms at equilibrium when the A-site cation is smaller than Dy (although larger cations may still form this polymorph through quenching of a high temperature phase). Although the cations are randomly arranged over long length scales, neutron diffraction experiments have shown pronounced diffuse scattering in the cubic phases and it has been proposed that these materials display local pyrochlore ordering[33,34]. Previous studies have shown that all defect fluorite A_2TiO_5 compositions show antiferromagnetic interactions even in those whose parent pyrochlore is normally ferromagnetic (*e.g.*, $Ho_2Ti_2O_7$, $Dy_2Ti_2O_7$, $Yb_2Ti_2O_7$)[32]. For rare-earth cations larger than Ho, an orthorhombic structure forms (*Pnma*) at equilibrium in which there are three distinct cation sites, and no mixed occupancy between cations (Fig. 1c). The pyrochlore, defect fluorite, and orthorhombic, "215"-type structures all belong to the broader family of fluorite derivative structures but significantly differ with respect to the arrangement of magnetic atoms. Specifically, all three structure-types contain networks of rare-earth tetrahedra. Unlike the pyrochlore, which is comprised of corner-sharing tetrahedra, the defect fluorite and orthorhombic "215"-type variants contain edge sharing tetrahedra. The orthorhombic variant is significantly more complex, with interwoven coplanar, triangular lattice-like layers (see blue lines in Fig. 1c), the endpoints of which form the caps of the tetrahedral network. Given the stoichiometric relation of the "215"-type and defect fluorite polymorphs, it is not presently clear if the defect fluorite polymorphs may actually possess local ordering that significantly differs from the pyrochlore thereby altering their magnetic properties.

In this paper, we present experimental results characterizing such structural disorder and magnetic properties on cubic Yb_2TiO_5, which we hope will serve as a benchmark for highly disordered $Yb_2Ti_2O_7$.

II. METHODS

A. Sample Synthesis

Stoichiometric ratios of Yb_2O_3 and TiO_2 were mixed in a mortar and pestle in an acetone slurry and cold pressed into a rod using a hydraulic press. The sample rod was heated in a box furnace to 1400 °C and subsequently heated in an infrared image furnace with a pulling rate of 30 mm/h under 3 atmosphere oxygen pressure. The resultant polycrystalline sample was ground into a fine powder and checked for purity using a laboratory x-ray powder diffractometer.

B. Structural Characterization

1. *X-ray Diffraction*

X-ray diffraction (XRD) measurements were performed at the Advanced Photon Source at the 6-ID-D beamline. Samples were measured in transmission mode, with the sample held in flat plate Cu holders using 100 keV X-rays at room temperature. Rietveld refinement was performed using the Fullprof software[35]. The background from an empty sample holder was subtracted and the remaining diffuse background was fit with a 4-coefficient polynomial function.

2. Neutron Total Scattering

Neutron total scattering experiments were performed at the Nanoscale Ordered Materials Diffractometer (NOMAD) beamline at the Spallation Neutron Source at Oak Ridge National Laboratory[36]. Polycrystalline Yb_2TiO_5 powder was loaded into 3 mm diameter quartz capillaries to a height of approximately 1 cm. Samples were exposed to the neutron beam at room temperature for one hour. An identical empty capillary was also measured for one hour for background subtraction.

The total scattering structure function $S(Q) - 1$ was obtained by normalizing scattering intensity from the sample to that of a vanadium standard. The reduced pair distribution function (PDF) was calculated using the Fourier transform of $S(Q) - 1$:

$$G(r) = \frac{2}{\pi} \int_{Q_{min}}^{Q_{max}} Q[S(Q) - 1]\sin(Qr)dQ, \qquad (1)$$

where Q is the scattering vector which is defined as $Q = 4\pi/\lambda\sin(\theta)$ in which λ and θ are the neutron wavelength and scattering angle, respectively. A value of 0.1 $Å^{-1}$ and 31.4 $Å^{-1}$ was used for Q_{min} and Q_{max} respectively in the Fourier transform. To exclude the effects of artificial ripples on data analysis, $S(Q) - 1$ was multiplied by a Lorch function[37] prior to the transformation. PDF data was refined using PDFgui software[38].

C. Magnetic Characterization

All *dc* susceptibility and magnetization measurements were taken using a commercial superconducting quantum interference device (SQUID) magnetometer. The *ac* susceptibility measurements were taken at the National High Magnetic Field Laboratory at Florida State University using the conventional mutual inductance technique at frequencies from 40 to 1000 Hz.

Inelastic neutron scattering measurements were performed at the time-of-flight disk chopper spectrometer (DCS) at NIST center for neutron research[39]. Monochromatic neutrons with a wavelength of 5 Å were used to measure magnetic excitations while 1.8 Å neutrons were used to investigate magnetic Bragg reflections in the elastic band. Around 5 g of powder sample was loaded into a copper can and was cooled down to the lowest measurement temperature of 60 mK with a dilution refrigerator. Scattering data from an empty copper can measured at 4 K was used to do the background subtraction. The data processing were performed using the DAVE software package[40].

III. RESULTS

A. Structural Characterization

1. Average Structure

The Bragg reflections in the X-ray diffraction (XRD) pattern for Yb_2TiO_5 can be indexed using $Fm\bar{3}m$ symmetry, which is characteristic of the cubic, defect fluorite structure (Fig. 2, prominent Bragg reflections are labeled). Rietveld refinement of the diffraction pattern using this model reproduces the measured data reasonably well with a goodness-of-fit parameter (R_{wp}) of 12.7. This model is characteristic of the average (long-range) structure in which Yb and Ti atoms share mixed occupancy of a single site (4*a*) and an oxygen vacancy randomly occupies $\frac{1}{6}$ of anion sites (8*c*). The unit cell parameter a was determined to be 5.0944(5) Å, which agrees well with previous studies[41]. Despite a reasonable fit to the data, there is noticeable diffuse scattering in the XRD pattern that cannot be reproduced with a defect fluorite model and is suggestive of local ordering of another phase. This diffuse scattering is dramatically increased in the neutron diffraction (ND) pattern suggesting that a significant portion of the local ordering is restricted to the oxygen sublattice. The position of the diffuse peaks in the diffraction patterns is in the area that one would expect to see superstructure peaks from the pyrochlore structure. For this reason, it was previously believed that these materials exhibit local, nanomeric pockets of pyrochlore-type ordering and only appear disordered over longer length scales[33,34,41,42]. This is not the case, however, for disordered Yb_2TiO_5 as we show in Section III A.2.

2. Local Structure

Recent studies utilizing methods to probe the local structure (*i.e.* neutron total scattering and Raman spectroscopy) have found that many related materials with long range defect fluorite ordering possess local orthorhombic ordering rather than pyrochlore ordering[43–45]. We performed pair distribution function (PDF) analysis from neutron total scattering data to test these different proposals as to the origin of the diffuse scattering in Yb_2TiO_5. While the cubic, defect fluorite structure ($Fm\bar{3}m$ space group) accurately represents the average structure, small-box refinement of the neutron PDF shows that this model is not valid locally (Fig. 3a, top). While the entire r-range is modeled poorly, it is particularly evident by examining the nearest neighbor coordination shells, especially Ti-O. Titanium and oxygen have contrasting neutron scattering lengths (-3.438 and 5.803 fm, respectively), which creates negative peaks in the PDF. While higher r Ti-O correlations convolute with positive correlations (such as

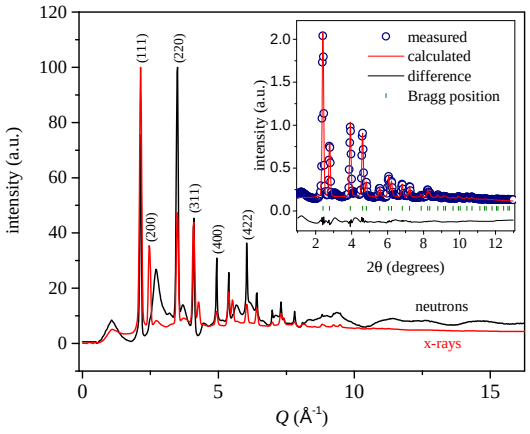

FIG. 2. (color online) X-ray and neutron diffraction pattern of Yb_2TiO_5 measured at room temperature (red and black lines respectively). Diffuse scattering is evident in both measurements but is much more pronounced in the neutron measurements. The average structure is consistent with the defect fluorite structure as evidenced by Rietveld refinement of the X-ray diffraction pattern (R_{wp} = 12.7, inset).

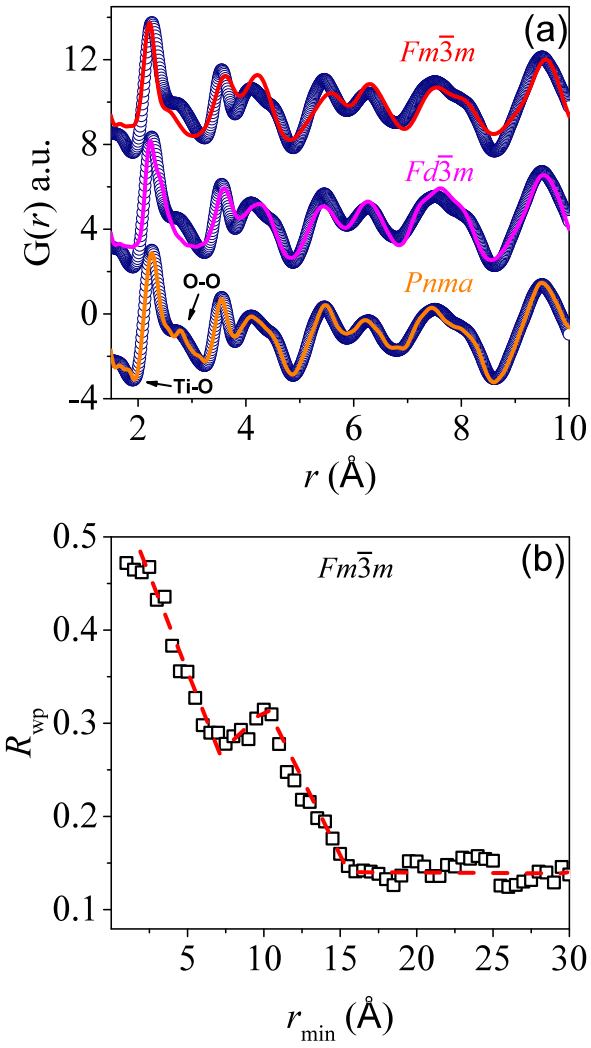

FIG. 3. (color online) (a) Neutron pair distribution function (PDF) of Yb_2TiO_5 measured at room temperature (open symbols) refined with various structural models (solid black line). The defect fluorite ($Fm\bar{3}m$, blue triangles) and defect pyrochlore ($Fd\bar{3}m$, red circles) models fit the data very poorly (R_{wp} = 0.477 and 0.306, respectively). The orthorhombic symmetry, characteristic of A_2TiO_5 stoichiometry with smaller A-site cations, reproduces the data well (R_{wp} = 0.111). (b) Goodness-of-fit parameter R_{wp} obtained from 'boxcar' refinement using the defect fluorite structure in which the fit range in incrementally shifted to higher r-values. The fit range was always 9 Å. The minimum r-value used for the fit range is shown on the x-axis. The fit is poor at low r-values but improves at higher r-values, eventually saturating above $r_{min} \approx 15$ Å.

Yb-O), the nearest neighbor Ti-O correlation is easily observable as the negative peak at ≈ 1.9 Å. This correlation is cancelled out in the disordered fluorite model, in which Ti and Yb are crystallographically equivalent, indicating the two cations are, in fact, locally distinct. The shoulder at ≈ 2.75 Å related to O-O coordination is also under-predicted with the defect fluorite model indicating that the oxygen sublattice is significantly more ordered. These discrepancies should not be surprising given the magnitude of the diffuse scattering in reciprocal space (Fig. 2). As mentioned previously, it has been proposed that many defect fluorite materials possess local pyrochlore order ($Fd\bar{3}m$ space group), however, this structure also fails to model the PDF representing the local structure (Fig. 3a, middle). In this model, Yb_2TiO_5 is often referred to as a "stuffed pyrochlore" and is more informatively written as $Yb_2(Ti_{1.33},Yb_{0.67})O_{6.67}$. Here, excess Yb^{3+} ions have been "stuffed" into the $A_2B_2O_7$ pyrochlore structure thereby altering the stoichiometry. It has been proposed that these additional Yb^{3+} ions replace Ti^{4+} in octahedral sites. The A-site (distorted cubic coordination) therefore remains fully occupied by Yb^{3+} ions while the B-site (octahedral coordination) is occupied by ≈ $\frac{1}{3}$ Yb^{3+} and $\frac{2}{3}$ Ti^{4+}. This structure also fails to model the nearest neighbor Ti-O peak as well as many other higher-r peaks.

As mentioned previously, Ln_2TiO_5 with lanthanides larger than Ho form an orthorhombic structure ($Pnma$ symmetry) and it is this structure that accurately models the neutron PDF for cubic Yb_2TiO_5 (Fig. 3a, bottom). The entire r-range that was included in the refinement (1 − 10 Å), including the nearest neighbor Ti-O peak as well as the O-O coordination, which were not captured with the cubic polymorphs, is modeled accurately. In this structure, Yb atoms fully occupy two distinct 4c sites that are 7-coordinated with oxygen, while Ti atoms occupy an additional 4c site that is 5-coordinated

with oxygen. This coexistence between orthorhombic and cubic polymorphs at different length scales is directly analogous to the weberite-type and fluorite relation described in Refs. [44] & [45]. The *Pnma* space group observed here is a non-isomorphic subgroup of the weberite-type symmetry that is present locally in disordered fluorite materials with $A_2B_2O_7$ and A_3BO_7 stoichiometry (*Ccmm* or $C222_1$). It is likely that orthorhombic local order in cubic, defect fluorite materials is more general behavior rather than an isolated phenomenon.

The magnitude and narrow width of the diffuse scattering in the diffraction patterns suggests that the correlation length of the local orthorhombic phase is quite large. To test the extent of the local order, the defect fluorite phase was refined at multiple r-ranges (*i.e.*, "boxcar" fitting). As shown in (Fig. 3b), the R_{wp} parameter initially decreases as the fit-range is increased. The R_{wp} increases between 7.5 Å and 10 Å, however, before decreasing again at higher r. The R_{wp} value saturates at $\approx$ 0.125 beyond R_{min} = 15 Å. This R_{wp} value is comparable to the value obtained from refining the low-r region with the orthorhombic structure. The general decrease in R_{wp} as the fit range is expanded is expected as atom-atom correlations become more average in nature rather than local. The saturation of the goodness-of-fit beyond 15 Å indicates that the structure is homogenous in this regime and can be completely described with defect fluorite ordering. This suggests that the local orthorhombic order is contained within local regions of less than 15 Å. This compares very favorably to neutron diffraction results from Lau *et al.*[34], which estimated the size of the locally ordered domains in Yb_2TiO_5 to be approximately 20 Å using the widths of the diffuse peaks. It is unclear whether the increase in R_{wp} between 7.5 and 10 Å has a physical origin or is an artifact from refinement. Multiple attempts were made to try to *not* reproduce this increase (*e.g.*, varying the width of the fit-range, changing the order of the boxcar refinement, *etc.*) but they were unsuccessful. It could possibly indicate a "period" of structural modulations but we believe that this increase is more likely due to the $Fm\bar{3}m$ and *Pnma* models being more similar in this range.

B. Magnetic Characterization

1. *dc and ac Susceptibility*

The *dc* susceptibility measurements show no evidence of a magnetic transition in our sample down to 2 K (Fig. 4). The Curie-Weiss law reproduces the measured susceptibility well from 2 − 20 K indicating paramagnetic behavior. The Curie-Weiss temperature, θ_{CW}, obtained from the fit was −3.18(3) K, which suggests antiferromagnetic interactions. The effective magnetic moment, μ_{eff} for each Yb^{3+} ion was evaluated to be 3.116(9) μ_B using the Curie constant from the fit. These values are in agreement with a previous study by Lau *et al.*[32] in which

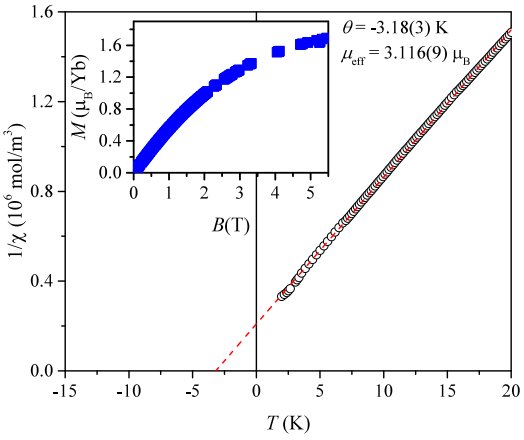

FIG. 4. (color online) Inverse *dc* susceptibility, χ_{dc}, (open black circles) as a function of temperature for Yb_2TiO_5.The Curie-Weiss law fits the data well (dashed red line) resulting in a Curie-Weiss temperature, θ_{CW}, of -3.18(3) K. The effective magnetic moment was evaluated to be 3.145(2) μ_B using the Curie constant from the fit. Magnetization measurements saturate below the moment of free Yb^{3+} (inset).

θ_{CW} and μ_{eff} were found to be −4.1(2) K and 3.71(5) μ_B respectively over the same fit range. The magnetization curve is not fully saturated at 6 T (Fig. 4 inset), around 1.6 - 1.7 μ_B, which is far below the expected moment for free Yb^{3+} ions (4.54 μ_B), suggesting that spins are highly anisotropic. Similar saturation was observed by Lau *et al.* for cubic Yb_2TiO_5[32] and this is also consistent with a previous magnetization study by Bramwell *et al.*[46] on $Yb_2Ti_2O_7$ pyrochlore. It suggests that Yb_2TiO_5 acts as an effective spin-1/2 system with well isolated higher crystal-electric-field (CEF) levels similar to that of $Yb_2Ti_2O_7$, whose CEF ground state wavefunctions contain major J_z = +/-1/2 components.[47]. Although not directly probed in the current study, this consistency is interesting considering the local structure of Yb_2TiO_5 is analogous to the average structure of orthorhombic A_2TiO_5 rather than the pyrochlore. It was previously shown that magnetization measurements of Dy_2TiO_5 saturated at a significantly higher moment than its cubic $Dy_2Ti_2O_7$ counterpart[48]. This was explained by the differing magnetic sublattices in the two compositions; Dy^{3+} ions occupy a single site in $Dy_2Ti_2O_7$ whereas they occupy two crystallographically distinct sites in Dy_2TiO_5, one of which does not have strong uniaxial symmetry. Based on the saturation in magnetization measurements, along with powder neutron diffraction measurements, it was suggested that the two Dy atoms have Ising and Heisenberg-like spins, respectively. In contrast our magnetization measurements of Yb_2TiO_5 in the current study do not suggest such a phenomenon as both spins appear anisotropic.

The real part of the *ac* susceptibility measured at 40

Hz shows a broad peak centered at 0.33 K [Fig. 5a]. This peak is frequency dependent and shifts to higher temperature with increasing frequency indicative of a relaxation process that is possibly related to a spin freezing/glassy transition. This behavior is quantitatively similar to that of $Yb_2Ti_2O_7$, where a weak frequency dependent χ'_{ac} is observed[49,50]. However, the imaginary part of the *ac* susceptibility shows much stronger frequency dependence than that of $Yb_2Ti_2O_7$. The frequency response of χ''_{ac} in the present study displays Arrhenius dependence ((Fig. 5a (inset)) with an activation energy of 2.51(5) meV (29.1(6) K). This activation energy is somewhat large but still reasonable and actually agrees very well with a previous study on powder $Ho_2Ti_2O_7$ and $Ho_2Sn_2O_7$ spin-ices (27.5 K and 19.6 K respectively) over the same temperature regime[51]. This agreement is actually quite surprising given the differences in local structure, magnetic moment, and anisotropy between the Ho-containing pyrochlores and Yb_2TiO_5 in the present study. However, it should also be noted that a detailed study on single-crystalline $Ho_2Ti_2O_7$ with careful corrections for demagnetization produced a smaller activation energy (10.7 K)[52]. Measurements under an applied magnetic field have the opposite effect (Fig. 5b) and shift the transition to lower temperatures (inset). This is distinct from spin-ice and would normally be suggestive of a simple spin glass, however, inelastic neutron scattering data reveal more complex behavior (discussed below).

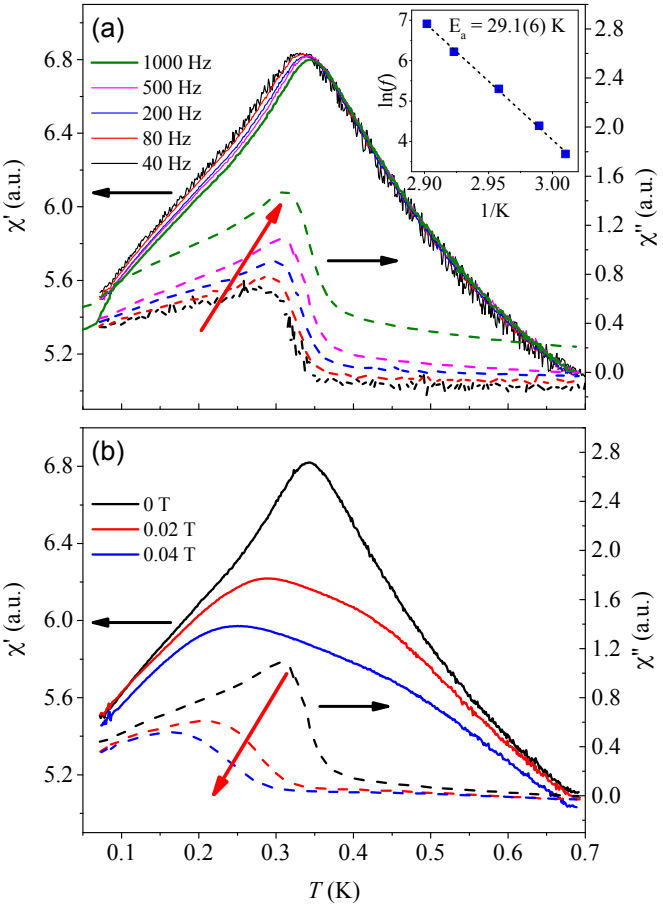

FIG. 5. (color online) (a) Frequency dependence of the real (χ', solid lines) and imaginary (χ'', dashed lines) part of *ac* susceptibility (left and right axes respectively) as a function of temperature for Yb_2TiO_5. The peak in χ' shifts to higher T with Arrhenius dependence as frequency is increased (inset). The activation energy extracted from the fit to the Arrhenius equation is 2.51(5) meV (dashed black line). (b) Field dependence of the real (χ', solid lines) and imaginary (χ'', dashed lines) part of *ac* susceptibility (left and right axes respectively) as a function of temperature for Yb_2TiO_5. The peak in χ' shifts to lower T as the applied field is increased (inset).

2. *Inelastic Neutron Scattering*

A zone of high intensity is readily apparent in the inelastic neutron scattering data (λ = 5 Å) from $|Q| \approx 0.6-1.4$ Å^{-1} at 5 K that is not separated from the elastic scattering band (Fig. 6a). This intensity increases when the temperature is lowered to 60 mK (Fig. 6b), indicating that it is magnetic in origin. There is again no visible separation between this excitation and the elastic scattering band suggesting a gapless excitation. Under an applied field of 2 T, a slight separation is visible that increases as the field is increased (Fig. 6c−d). At 4T there is a clear energy gap.

The Q-dependence of the excitation was obtained by integrating the data of the elastic band ($-0.05 \leq E \leq 0.05$ meV) of the inelastic neutron scattering data (λ = 5 Å) was performed to investigate the magnetic transition observed from *ac* susceptibility data (Fig. 7). A difference curve between the diffraction patterns taken at 60 mK and 5 K shows no evidence of magnetic Bragg peaks but instead a very broad, diffuse feature indicating short range magnetic order rather than long range (Fig. 7a). This is most apparent at low |Q| in which negative intensities of the difference curve are found, due to the subtraction of the paramagnetic scattering at 5 K. Data taken with 1.8 Å neutrons also show no evidence of zero-field magnetic Bragg peaks (not shown). This indicates that, unlike $Yb_2Ti_2O_7$ and $Yb_2Sn_2O_7$, the peak observed in the *ac* susceptibility data arises from a spin-glass type transition rather than long range order. This should not necessarily be surprising, as $Yb_2Ti_2O_7$ is already sensitive to very small amounts of structural disorder and the cations in Yb_2TiO_5 are completely disordered over long length scales. The structural heterogeneity with local orthorhombic and long-range cubic order further complicates mechanisms for a transition to long range order.

A Q-resolved Bragg peak forms at $|Q| \approx 2.1$ Å^{-1} under the presence of a 2 T magnetic field that continues growing in intensity up to 4 T (only 4T data is shown in Fig. 7b). This corresponds to the (111) peak of the average, defect-fluorite structure. Likewise, when using 1.8 Å neutrons, we observe an increase in the intensity of the (200) Bragg peak as well (inset). This is analogous

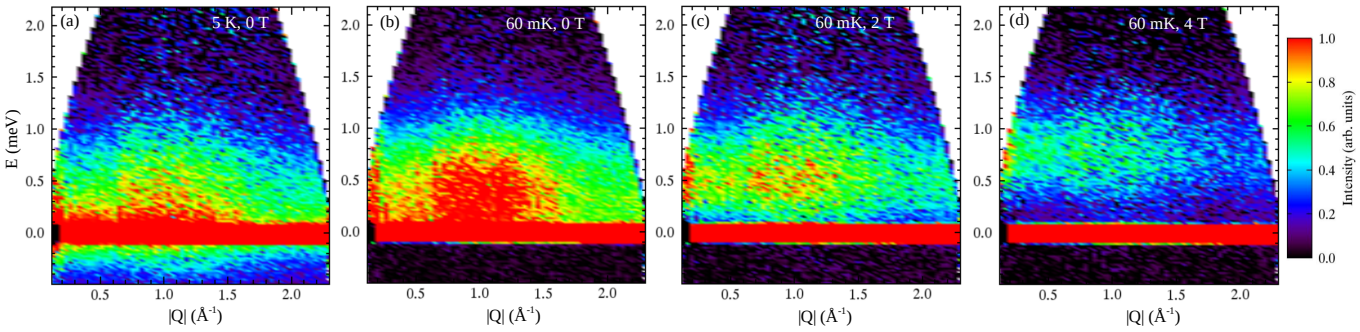

FIG. 6. (color online) Contour maps of the powder averaged inelastic neutron scattering spectrum of Yb_2TiO_5 ($\lambda = 5$ Å). Panel (a) shows the zero-field spectrum at 5K while panels (b)−(d) show spectra at 60 mK under various field strengths. A gapless excitation centered at $|Q| \approx 1$ Å^{-1} is evident at 60 mK under zero field [panel (b)]. An energy gap forms under applied magnetic field (panels (c)−(d)).

to what was observed by Dun *et al.*[53] on antiferromagnetic $Yb_2Ge_2O_7$ pyrochlore under an applied magnetic field. It was determined that above a critical applied field, H_c, $Yb_2Ge_2O_7$ enters a spin polarized state, where the observed neutron diffraction pattern can be fitted with a splayed ferromagnetic model. Interestingly, in the present study, there is also a change in the diffuse scattering which becomes more localized in the area of the (111) peak (denoted by an arrow in Fig. 6). This diffuse scattering, which remains present even under a 4 T magnetic field, indicates the coexistence of short and long range magnetic order and a strong tendency of spin disorder in Yb_2TiO_5. The magnetic Bragg peaks indicate $\mathbf{k} = 0$ order in which the component of the spin moment along the direction of the field display ferromagnetic order (spin polarized), while the component that is orthogonal to the field is only short range ordered. This behavior is likely rooted in the differing average and local structural order.

The Q-dependence of the excitation band was obtained by integrating the inelastic signals from E = 0.2−1.5 meV (Fig. 8a). There are two zones of high intensity centered at $|Q| \approx 0$ and $|Q| \approx 1$ Å. This suggests both ferromagnetic and antiferromagnetic components of spin-spin correlations which could arise from anisotropic exchange interactions similar to $Yb_2Ti_2O_7$[8]. The energy dependence of the $|Q| \approx 1$ Å^{-1} signal is obtained by integrating from 0.5 Å^{-1} to 1.5 Å^{-1} of the spectrum in Fig. 8b. As the magnetic field is increased, the spectral weight does not explicitly shift to higher energy as would be expected for a spin-wave excitation under magnetic fields. Rather, the spectral weight at low energy decreases while it is unaffected at high energies, which is again suggestive of a local excitation. This is in sharp contrast to the spin wave excitations of $Yb_2Ti_2O_7$ under high fields where the spectrum shifts to higher energies with increasing fields, due to the Zeeman term[8]. Furthermore, this excitation is not coming from thermal fluctuations, as it gets stronger with decreasing temperature and there is no intensity on the energy gain (negative energy) side at 60 mK. Given that there is no long range magnetic correlations (and only

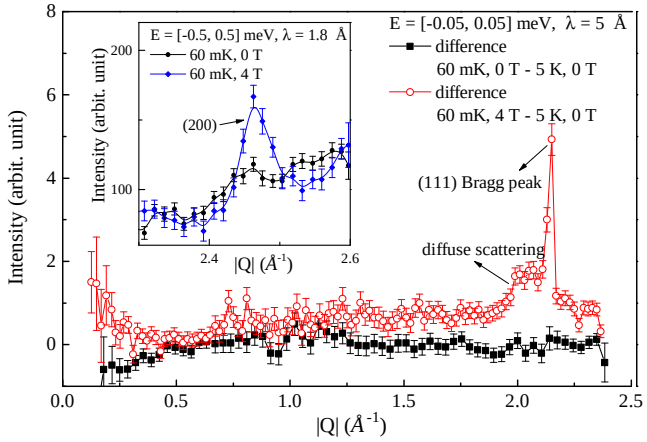

FIG. 7. (color online) The elastic neutron scattering data by integrating within $-0.05 \leq E \leq 0.05$ meV ($\lambda = 5$ Å). There is little difference in the data from 5 K to 60 mK under zero applied field (black squares) indicating the lack of long range magnetic order. The intensity of the (111) and (200) Bragg peaks **(inset) increase under applied magnetic field indicating a transformation to a spin-polarized, long-range magnetic ordered state (red squares). There is an additional diffuse peak that emerges around $|Q| \approx$ 2 Å indicating that short range order is still present in the presence of a 4 T field. Error bars represent one standard deviation determined assuming Poisson statistics.**

partial long range structural correlations), this excitation is almost certainly of local character (*e.g.*, a monopole-like single spin flip in spin-ice) rather than a long range collective mode (*e.g.*, spin wave).

IV. DISCUSSION

Given the large amount of disorder present in Yb_2TiO_5, one might expect that the lack of long range magnetic order and the presence of frequency dependence in *ac* susceptibility data points to a traditional spin glass

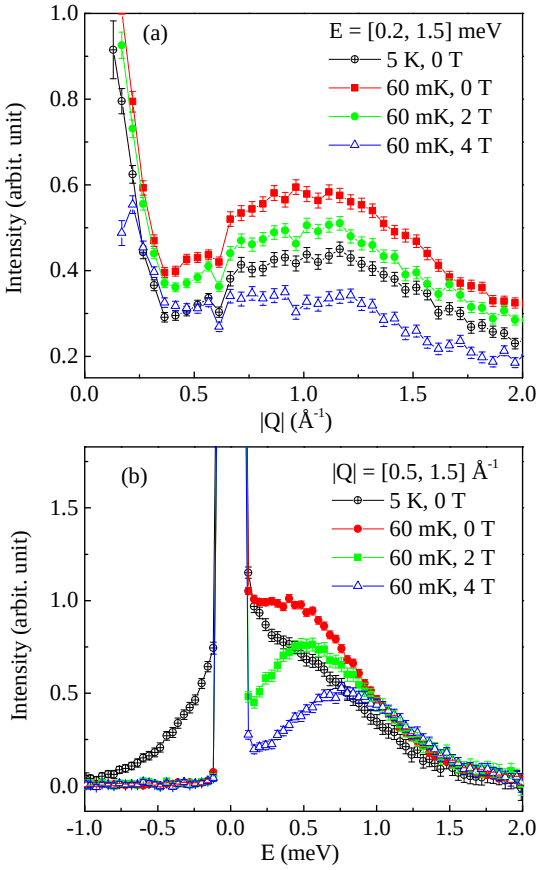

FIG. 8. (color online) (a) Q-dependence of inelastic neutron scattering spectra (Fig. 6) from integrating within E = 0.2−1.5 meV. The high intensity position of the excitation does not change as a function temperature or applied field. (b) Energy-dependence of inelastic neutron scattering data in Fig. 6 from integrating 0.5−1.5 Å^{-1}.

system. The large inelastic over elastic spectrum weight ratio can also be explained by a spin glass where 2/3 of the spectrum weight should lie in the inelastic channel even all the spins remain static, given the effective spin-1/2 nature of Yb^{3+}[54]. However, there are several features in the data that suggest otherwise. First, we note that the apparent disorder in Yb_2TiO_5 primarily pertains to long length scales; the local structure remains ordered with a correlation length up to 15 Å. While 15 Å is still considered quite "local" from a structural context, this ordered domain is quite significant for magnetic interactions and spin correlations. Second, due the random nature of the frozen state of spin-glasses, they often do not display simple thermally activated (Arrhenius) frequency dependence that we've shown to exist here. Analogous to structural glasses, spin-glasses often display a cooperative, dynamic liquid-glass transition (*i.e.* Vogel-Fulcher) in which attempts at fitting Arrhenius behavior result in unphysical parameters[4,55].

Finally, it is noteworthy that the gapless excitation in Yb_2TiO_5 is somewhat unexpected for a traditional spin glass. Spectral weight in traditional spin glasses is typically well separated from the elastic band from, for example, crystal-field excitations.[56–58]. The signal at zero field in the present study, however, is qualitatively similar to previous studies on Yb-based pyrochlores, $Yb_2Ti_2O_7$, $Yb_2Sn_2O_7$, and $Yb_2Ge_2O_7$[14,18,59,60]. In all cases, a low-temperature, gapless excitation was observed under zero-field with a pocket of high intensity centered at $|Q| \approx 1$ Å^{-1}. Therefore, it is possible, even with local-structural disorder presented in Yb_2TiO_5, the system remains a quantum magnet with continuum behavior. It should be noted, however, that the inelastic spectra are not identical between the 227 and 215 variants. In particular, the spectral weight is most intense at $|Q| = 1$ for Yb_2TiO_5 in the present study, whereas it is more evenly distributed between $|Q| = 0$ and $|Q| = 1$ for $Yb_2Ti_2O_7$[14].

Actually, materials with significant disorder effects (*e.g.*, site-mixing, bond randomness) have been largely omitted previously for studying their ground states since disorder is thought to suppress long-range quantum entanglement. It is becoming more clear, however, that the effect of disorder on frustrated magnetism is more complicated that previously thought. For example, it is proposed that the quantum spin liquid-like behavior in the triangular lattice antiferromagnet $YbMgGaO_4$ is possibly related to cation site-mixing (albeit between nonmagnetic Mg^{2+} and Ga^{3+} cations) which cause local distortions to YbO_6 octahedra[61–63]. Another example is found in the recently studied Yb-based tripod kagome lattice compounds where severe site-disorder in $Zn_2Yb_3Sb_3O_{14}$ fully destroyed the long-rang order in $Mg_2Yb_3Sb_3O_{14}$ and introduce some intriguing quantum behaviors in the susceptibility and specific heat[64]. The Yb_2TiO_5 studied here provide another example where disorder effect in spin-1/2 system might play an important role enhancing quantum fluctuations, with the advantages that the local disorder is better understood. Thus a more comprehensive understanding of disorder is needed to illustrate its effect on quantum magnets.

V. CONCLUSIONS

In summary, the structural and magnetic properties of fully stuffed $Yb_2Ti_2O_7$ pyrochlore (Yb_2TiO_5) have been investigated using a combination of neutron total scattering, magnetic susceptibility and inelastic neutron scattering. Yb_2TiO_5 is a complex system in which differing local and long-range interactions play a role in magnetic properties. PDF refinement revealed that stuffing the pyrochlore structure with excess Yb^{3+} ions transforms the local crystal structure to more closely resemble orthorhombic Ln_2TiO_5 polymorphs, despite the average structure remaining cubic. Under zero-field, Yb_2TiO_5 remains in a disordered state with antiferromagnetic interactions. Low-temperature *ac* susceptibility measurements show evidence of a short range magnetic transition between 0.3 and 0.35 K that varies with frequency and

displays Arrhenius dependence. A gapless spin excitation is evident at low temperatures which gives way to a gapped excitation under modest magnetic fields. This gapped excitation corresponds to the onset of a partially spin polarized state in which there is a coexistence between short- and long-range magnetic correlations.

ACKNOWLEDGEMENTS

J.S. and S.J. acknowledge support from The University of Tennessee Office of Research's Organized Research Unit program. Z.L.D. and H.D.Z. acknowledge support from the National Science Foundation (NSF) Contract No. NSF-DMR- 1350002. A portion of this research used the NOMAD beamline at the Spallation Neutron Source, a DOE Office of Science User Facility operated by the Oak Ridge National Laboratory. A portion of this work was performed at the National High Magnetic Field Laboratory, which is supported by NSF Cooperative Agreement No. DMR-1157490 and the State of Florida. This work utilized facilities supported in part by the National Science Foundation under Agreement No. DMR-1508249. This research used resources of the Advanced Photon Source, a U.S. Department of Energy (DOE) Office of Science User Facility operated for the DOE Office of Science by Argonne National Laboratory under Contract No. DE-AC02-06CH11357.

* hzhou10@utk.edu

[1] J. S. Gardner, M. J. P. Gingras, and J. E. Greedan, Reviews of Modern Physics **82**, 53 (2010).

[2] M. J. Harris, S. T. Bramwell, D. F. McMorrow, T. Zeiske, and K. W. Godfrey, Physical Review Letters **79**, 2554 (1997).

[3] A. P. Ramirez, A. Hayashi, R. J. Cava, R. Siddharthan, and B. S. Shastry, Nature **399**, 333 (1999).

[4] S. T. Bramwell and M. J. P. Gingras, Science **294**, 1495 (2001).

[5] C. Castelnovo, R. Moessner, and S. L. Sondhi, Nature **451**, 42 (2008).

[6] S. T. Bramwell, S. R. Giblin, S. Calder, R. Aldus, D. Prabhakaran, and T. Fennell, Nature **461**, 956 (2009).

[7] J. A. Hodges, P. Bonville, A. Forget, A. Yaouanc, P. Dalmas de Reotier, G. Andre, M. Rams, K. Krolas, C. Ritter, P. C. M. Gubbens, C. T. Kaiser, P. J. C. King, and C. Baines, Physical Review Letters **88**, 077204 (2002).

[8] K. A. Ross, L. Savary, B. D. Gaulin, and L. Balents, Physical Review X **1**, 021002 (2011).

[9] J. D. Thompson, P. A. McClarty, D. Prabhakaran, I. Cabrera, T. Guidi, and R. Coldea, ArXiv e-prints Phys. Rev. Lett. **119**, 057203 (2017).

[10] L. D. C. Jaubert, O. Benton, J. G. Rau, J. Oitmaa, R. R. P. Singh, N. Shannon, and M. J. P. Gingras, Physical Review Letters **115**, 267208 (2015).

[11] J. Robert, E. Lhotel, G. Remenyi, S. Sahling, I. Mirebeau, C. Decorse, B. Canals, and S. Petit, Physical Review B **92**, 064425 (2015).

[12] H. Yan, O. Benton, L. Jaubert, and N. Shannon, Physical Review B 95, 094422 (2017).

[13] H. W. J. Blote, R. F. Wielinga, and W. J. Huiskamp, Physica **43**, 549 (1969).

[14] K. A. Ross, J. P. C. Ruff, C. P. Adams, J. S. Gardner, H. A. Dabkowska, Y. Qiu, J. R. D. Copley, and B. D. Gaulin, Physical Review Letters **103**, 227202 (2009).

[15] J. S. Gardner, G. Ehlers, N. Rosov, R. W. Erwin, and C. Petrovic, Physical Review B **70**, 180404 (2004).

[16] K. A. Ross, L. R. Yaraskavitch, M. Laver, J. S. Gardner, J. A. Quilliam, S. Meng, J. B. Kycia, D. K. Singh, T. Proffen, H. A. Dabkowska, and B. D. Gaulin, Physical Review B **84**, 174442 (2011).

[17] Y. Yasui, M. Soda, S. Iikubo, M. Ito, M. Sato, N. Hamaguchi, T. Matsushita, N. Wada, T. Takeuchi, N. Aso, and K. Kakurai, Journal of the Physical Society of Japan **72**, 3014 (2003).

[18] J. Gaudet, K. A. Ross, E. Kermarrec, N. P. Butch, G. Ehlers, H. A. Dabkowska, and B. D. Gaulin, Physical Review B **93**, 064406 (2016).

[19] A. Scheie, J. Kindervater, S. Saubert, C. Duvinage, C. Pfleiderer, H. J. Changlani, S. Zhang, L. Harriger, K. Arpino, S. M. Koohpayeh, O. Tchernyshyov, and C. Broholm, Physical Review Letters 119, 127201 (2017).

[20] V. Pecanha-Antonio, E. Feng, Y. Su, V. Pomjakushin, F. Demmel, L.J. Chang, R.J. Aldus, Y. Xiao, M.R. Lees, and T. Bruckel, ArXiv e-prints, arXiv:1709.01013v1

[21] L. J. Chang, S. Onoda, Y. X. Su, Y. J. Kao, K. D. Tsuei, Y. K. Yasui, K. Kakurai, and M. R. Lees, Nature Communications **3**, 992 (2012).

[22] K. E. Arpino, B. A. Trump, A. O. Scheie, T. M. McQueen, and S. M. Koohpayeh, Physical Review B **95**, 094407 (2017).

[23] A. Mostaed, G. Balakrishnan, M. R. Lees, Y. Yasui, L. J. Chang, and R. Beanland, Physical Review B **95**, 094431 (2017).

[24] A. Yaouanc, P. D. Dalmas de Reotier, C. Marin, and V. Glazkov, Physical Review B **84**, 172408 (2011).

[25] K. A. Ross, T. Proffen, H. A. Dabkowska, J. A. Quilliam, L. R. Yaraskavitch, J. B. Kycia, and B. D. Gaulin, Physical Review B **86**, 174424 (2012).

[26] J. Snyder, S. Slusky, R. J. Cava, and P. Schiffer, Physical Review B **66**, 064432 (2002).

[27] J. Snyder, B. G. Ueland, A. Mizel, J. S. Slusky, H. Karunadasa, R. J. Cava, and P. Schiffer, Physical Review B 70, 184431 (2004).

[28] G. Ehlers, J. S. Gardner, C. H. Booth, M. Daniel, K. C. Kam, A. K. Cheetham, D. Antonio, H. E. Brooks, A. L. Cornelius, S. T. Bramwell, J. Lago, W. Haeussler, and N. Rosov, Physical Review B 73, 174429 (2006).

[29] J. Gaudet, A. M. Hallas, D. D. Maharaj, C. R. C. Buhariwalla, E. Kermarrec, N. P. Butch, T. J. S. Munsie, H. A. Dabkowska, G. M. Luke, and B. D. Gaulin, Physical Review B 94, 060407 (2016).

[30] A. Keren, J. S. Gardner, G. Ehlers, A. Fukaya, E. Segal, and Y. J. Uemura, Physical Review Letters 92, 107204 (2004).

[31] G. C. Lau, R. S. Freitas, B. G. Ueland, B. D. Muegge, E. L. Duncan, P. Schiffer, and R. J. Cava, Nature Physics **2**,

249 (2006).
[32] G. C. Lau, B. D. Muegge, T. M. McQueen, E. L. Duncan, and R. J. Cava, Journal of Solid State Chemistry **179**, 3126 (2006).
[33] G. C. Lau, R. S. Freitas, B. G. Ueland, M. L. Dahlberg, Q. Huang, H. W. Zandbergen, P. Schiffer, and R. J. Cava, Physical Review B **76**, 054430 (2007).
[34] G. C. Lau, T. M. McQueen, Q. Huang, H. W. Zandbergen, and R. J. Cava, Journal of Solid State Chemistry **181**, 45 (2008).
[35] J. Rodriguez-Carvajal, ILL (unpublished) (2009-2012).
[36] J. Neuefeind, M. Feygenson, J. Carruth, R. Hoffmann, and K. Chipley, Nucl. Instrum. Methods Phys. Res., Sect. B **287** (2012).
[37] A.K. Soper and E.R. Barney, J. Appl. Cryst. **45** (2012).
[38] C. L. Farrow, P. Juhas, J. W. Liu, D. Bryndin, E. S. Bozin, J. Bloch, T. Proffen, and S. J. L. Billinge, Journal of Physics-Condensed Matter **19**, 335219 (2007).
[39] J. R. D. Copley and J. C. Cook, Chemical Physics **292**, 477 (2003).
[40] R. T. Azuah, L. R. Kneller, Y. M. Qiu, P. L. W. Tregenna-Piggott, C. M. Brown, J. R. D. Copley, and R. M. Dimeo, Journal of Research of the National Institute of Standards and Technology 114, 341 (2009).
[41] R. D. Aughterson, G. R. Lumpkin, M. d. L. Reyes, N. Sharma, C. D. Ling, B. Gault, K. L. Smith, M. Avdeev, and J. M. Cairney, Journal of Solid State Chemistry **213**, 182 (2014).
[42] M. L. Sanjuan, C. Guglieri, S. Diaz-Moreno, G. Aquilanti, A. F. Fuentes, L. Olivi, and J. Chaboy, Physical Review B **84**, 104207 (2011).
[43] C. L. Tracy, J. Shamblin, S. Park, F. Zhang, C. Trautmann, M. Lang, and R. C. Ewing, Physical Review B **94**, 064102 (2016).
[44] J. Shamblin, M. Feygenson, J. Neuefeind, C. L. Tracy, F. Zhang, S. Finkeldei, D. Bosbach, H. Zhou, R. C. Ewing, and M. Lang, Nat Mater **15**, 507 (2016).
[45] G. King, C. M. Thompson, J. E. Greedan, and A. Llobet, Journal of Materials Chemistry A **1**, 10487 (2013).
[46] S. T. Bramwell, M. N. Field, M. J. Harris, and I. P. Parkin, Journal of Physics-Condensed Matter 12, 483 (2000).
[47] J. Gaudet, D. D. Maharaj, G. Sala, E. Kermarrec, K. A. Ross, H. A. Dabkowska, A. I. Kolesnikov, G. E. Granroth, and B. D. Gaulin, Physical Review B 92, 134420 (2015).
[48] J. Shamblin, S. Calder, Z. Dun, M. Lee, E. S. Choi, J. Neuefeind, H. Zhou, and M. Lang, Physical Review B **94**, 024413 (2016).
[49] E. Lhotel, S. R. Giblin, M. R. Lees, G. Balakrishnan, L. J. Chang, and Y. Yasui, Physical Review B **89**, 224419 (2014).
[50] Z. L. Dun, M. Lee, E. S. Choi, A. M. Hallas, C. R. Wiebe, J. S. Gardner, E. Arrighi, R. S. Freitas, A. M. Arevalo-Lopez, J. P. Attfield, H. D. Zhou, and J. G. Cheng, Physical Review B **89**, 064401 (2014).
[51] K. Matsuhira, Y. Hinatsu, K. Tenya, and T. Sakakibara, Journal of Physics-Condensed Matter **12**, L649 (2000).
[52] J. A. Quilliam, L. R. Yaraskavitch, H. A. Dabkowska, B. D. Gaulin, and J. B. Kycia, Physical Review B **83**, 094424 (2011).
[53] Z. L. Dun, X. Li, R. S. Freitas, E. Arrighi, C. R. Dela Cruz, M. Lee, E. S. Choi, H. B. Cao, H. J. Silverstein, C. R. Wiebe, J. G. Cheng, and H. D. Zhou, Physical Review B **92**, 140407 (2015).
[54] K. A. Ross, J. W. Krizan, J. A. Rodriguez-Rivera, R. J. Cava, and C. L. Broholm, Physical Review B **93**, 014433 (2016).
[55] C. Djurberg, P. Svedlindh, P. Nordblad, M. F. Hansen, F. Bodker, and S. Morup, Physical Review Letters **79**, 5154 (1997).
[56] G. Ehlers, J. E. Greedan, J. R. Stewart, K. C. Rule, P. Fouquet, A. L. Cornelius, C. Adriano, P. G. Pagliuso, Y. Qiu, and J. S. Gardner, Physical Review B **81**, 224405 (2010).
[57] D. K. Singh, J. S. Helton, S. Chu, T. H. Han, C. J. Bonnoit, S. Chang, H. J. Kang, J. W. Lynn, and Y. S. Lee, Physical Review B **78**, 220405 (2008).
[58] E. A. Goremychkin, R. Osborn, B. D. Rainford, R. T. Macaluso, D. T. Adroja, and M. Koza, Nature Physics **4**, 766 (2008).
[59] Z. L. Dun, E. S. Choi, H. D. Zhou, A. M. Hallas, H. J. Silverstein, Y. Qiu, J. R. D. Copley, J. S. Gardner, and C. R. Wiebe, Physical Review B **87**, 134408 (2013).
[60] A. M. Hallas, J. Gaudet, N. P. Butch, M. Tachibana, R. S. Freitas, G. M. Luke, C. R. Wiebe, and B. D. Gaulin, Physical Review B **93**, 100403 (2016).
[61] J. A. M. Paddison, M. Daum, Z. Dun, G. Ehlers, Y. Liu, M. B. Stone, H. Zhou, and M. Mourigal, Nature Physics **13**, 117 (2017).
[62] Y. Li, D. Adroja, R. I. Bewley, D. Voneshen, A. A. Tsirlin, P. Gegenwart, and Q. Zhang, Physical Review Letters **115**, 267208 (2017).
[63] Z. Zhu, P. A. Maksimov, S. R. White, A. L. Chernyshev, ArXiv e-prints, arXiv:1703.02971v2.
[64] Z. L. Dun, J. Trinh, M. Lee, E. S. Choi, K. Li, Y. F. Hu, Y. X. Wang, N. Blanc, A. P. Ramirez, H. D. Zhou, Phys. Rev. B **95**, 104439, (2017).